FULL PAPER

Ultrafast Carotenoid to Retinal Energy Transfer in Xanthorhodopsin Revealed by the Combination of Transient Absorption and Two Dimensional Electronic Spectroscopy

Francesco Segatta,[a,b] Itay Gdor,[c] Julien Réhault,[d] Simone Taioli,[a] Noga Friedman,[e] Mordechai Sheves,[e] Ivan Rivalta [f], Sanford Ruhman,*[c] Giulio Cerullo,*[g] and Marco Garavelli *[b]

Abstract: By comparing two-dimensional electronic spectroscopy (2DES) and Pump-Probe (PP) measurements on *xanthorhodopsin* (XR) and *reduced-xanthorhodopsin* (RXR) complexes, the ultrafast carotenoid-to-retinal energy transfer pathway is revealed, at very early times, by an excess of signal amplitude at the associated cross-peak and by the carotenoid bleaching reduction due to its ground state recovery. The combination of the measured 2DES and PP spectroscopic data with theoretical modelling allows a clear identification of the main experimental signals and a comprehensive interpretation of their origin and dynamics. The remarkable velocity of the energy transfer, despite the non-negligible energy separation between the two chromophores, and the analysis of the underlying transport mechanism, highlight the role played by the ground state carotenoid vibrations in assisting the process.

[a] Dr. F. Segatta, Dr. S. Taioli
European Center for Theoretical Studies in Nuclear Physics and Related Areas (ECT*-FBK)
38123 Trento, Italy
[b] Dr. F. Segatta, Prof. Dr. M. Garavelli
Department of Industrial Chemistry
University of Bologna
Viale Risorgimento 4, 40136, Bologna, Italy
E-mail: marco.garavelli@unibo.it
[c] Dr. I. Gdor, Prof. Dr. S. Ruhman
Department of Physical Chemistry
The Hebrew University
Jerusalem, 9190401, Istrael
E-mail: sandy@mail.huji.ac.il
[d] Dr. J. Réhault
Department für Chemie und Biochemie
University of Bern
Freiestrasse 3, 3012 Bern, Switzerland
[e] Dr. N. Friedman, Prof. Dr. M. Sheves
Department of Organic Chemistry
Weizmann Institute of Science
Rehovot 76100, Israel
[f] Dr. I. Rivalta
Laboratoire de Chimie UMR 5182
Université Lyon, ENS de Lyon, CNRS, Unversité Lyon 1
Allée d'Italie 46, FR-69342 Lyon, France
[g] Prof. Dr. G. Cerullo
Department of Physics
Politecnico di Milano
Piazza Leonardo da Vinci 32, 20133, Milano, Italy
E-mail: giulio.cerullo@fisi.polimi.it

Supporting information for this article is given via a link at the end of the document.

Introduction

Xanthorhodopsin (XR) of the extremely halophilic eubacterium Salinibacter ruber [1] is a light-driven transmembrane proton pump with two chromophores: an all-trans-retinal (RET), responsible for the proton transport function, and a C40 carotenoid (CAR) salinixanthin [2,3], which acts as a light-harvesting antenna. It represents one of the simplest photosynthetic protein complexes for the study of excitation energy transfer (EET): a perfect donor-acceptor pair, with the carotenoid bound to the protein in a 1:1 ratio.

The complex excited state energy levels structure of the salinixanthin CAR includes the bright S_2 state, responsible for the strong absorption in the blue-green spectral region, and a dark state, S_1, lower in energy and populated via S_2-to-S_1 internal conversion (IC) on a sub-picosecond timescale. The existence of additional dark excited states (e.g., the so-called S* state), located below the S_2 state, has also been proposed in previous studies [4, 5]. In the protein-bound RET, the reactive S_1 state is known to undergo isomerization from all-trans to 13-cis [6,7].

The resolved XR crystal structure [8] reveals a 46° angle between the two chromophores molecular axes, and a center to center distance of 11.7 Å. Steady-state spectroscopic studies [9,10] were performed on both XR system and $NaBH_4$-treated XR, so-called reduced-xanthorhodopsin (RXR). The $NaBH_4$ treatment blue-shifts the absorption energy of the RET, due to hydrogenation of the retinal Schiff base double bond, and prevents EET without significantly perturbing the CAR binding site. In both samples, well-resolved vibronic absorption bands of salinixanthin bound to XR are recorded [11] (Figure 1). Action spectra for proton transport [11,12] as well as fluorescence excitation spectra of the retinal chromophore [9] showed that light absorbed not only by the retinal but also by the carotenoid is employed for proton transport. Quantum yields of emission and energetic positioning of the chromophores states, indicate that the EET route should proceed from the extremely short-lived CAR S_2 state to the reactive retinal S_1. The efficiency of this process was estimated to be between 30% and 50% [9-12], suggesting an ultrafast EET process able to compete with the sub-picosecond CAR $S_2 \rightarrow S_1$ IC.

Femtosecond transient absorption studies [13-15] have been previously employed to directly investigate the dynamics of CAR→RET EET and CAR $S_2 \rightarrow S_1$ IC. They provide a further support to the postulated EET pathway as well as an estimate of the various IC and EET rates. Polivka et. al [14], showed that the difference of the normalized XR and RXR transient absorption

spectra at 1ps strictly resembles J/K state signals of bacteriorhodopsin; moreover, they observed that a persistent signal at 615 nm was present at very long time (t_2 > 20ps) in XR, while absent in RXR, explaining this difference as a signature of the RET K photoproduct. In the NIR, they also demonstrated that $S_2 \rightarrow S_{2n}$ excited state absorption (ESA) signals last for about 100 fs in XR and 130 fs in RXR (in line with the estimated ~30% of EET efficiency), and characteristic RET stimulated emission (SE) was only present in the XR sample. Additional evidence was provided by the studies of some of the present authors [13,15]: comparing PP experiments with different polarization it was possible to isolate sensitized RET signals in XR, appearing around 560 nm; the analysis of the K band anisotropy was also exploited to obtain an independent estimate of EET efficiency of ~32%. In the NIR, by comparing the relative intensities of S_1 evolution associated difference spectra (EADS), an estimate of EET efficiency around 35 ± 7% was obtained.

These studies, performed with 100-fs [14] and 70-fs [15] time resolution, provided a CAR S_2 lifetime of 70-100 fs and 110-130 fs for XR and RXR respectively. Measurements performed in the visible window [13] with sub-10-fs time resolution estimated it to be below 30 fs, in contrast with the NIR [14,15] results, but it was not clear if broadband ultrafast excitation leads to fundamentally different S_2 excited states, or that nonlinearities dominate the extreme time resolution experiments [15].

By spreading the signals along two frequency axes, time resolved two-dimensional electronic spectroscopy (2DES) allows to both decongest transient absorption spectra and follow the direct signal of an EET process [16-18]. This appears in the 2DES maps as a cross-peak between the two interacting chromophores, whose form and evolution in time allows direct probe of its dynamics. For instance, this technique has been successfully applied to track and time resolve EET processes in complex multichromophoric LH systems [16,19].

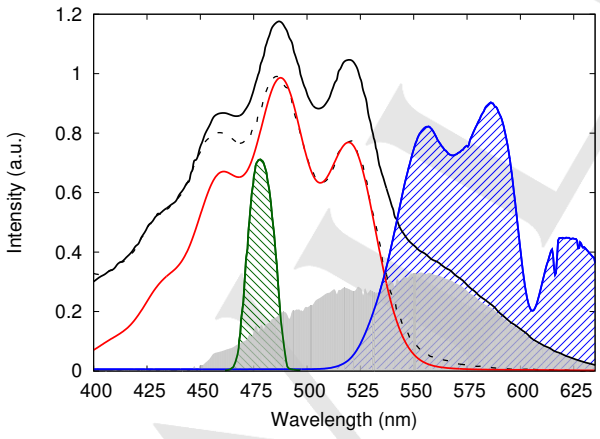

Figure 1. Experimental absorption spectra of XR (black solid line) and RXR (dashed line), together with their difference (grey filled curve), which reveals the RET absorption. The theoretical RXR absorption (red solid line) does not contain the reduced retinal contribution in the blue side of the spectrum. The spectra of the pulse used for the 2DES experiments (measured upstream of the sample, blue filled curve) and the pump pulse in the PP experiment (green filled curve) are also reported. The experimental absorption spectra were adapted from ref. 9.

However, support by theoretical modeling is also mandatory to interpret the signals and disentangle the different components observed, specifically when spectrally congested regions persist [20].

In the present study, we compare experimental 2DES maps and broadband PP spectra of XR and RXR systems with simulated RXR maps, aimed at finding signatures of the efficient CAR→RET EET and elucidating the nature of the underlying transport mechanism. 2DES measurements (performed with a sub-10-fs time resolution and at room temperature) confirm that the EET route occurs from the bright S_2 state of the CAR to the S_1 of the RET, clearly showing a EET related signature at the CAR-to-RET cross-peak. The comparison between 2DES and PP results, supported by theoretical arguments, allowed us to monitor the different processes that take place and follow their dynamics: in both samples, we observed the ultrafast CAR $S_2 \rightarrow S_1/S^*$ internal conversion, revealed by the disappearance of the S_2 SE and by the rise of $S_1 \rightarrow S_{1n}$ ($S^* \rightarrow S^*_n$) ESA, together with the CAR S_2 spectral diffusion and the S_1 vibrational cooling; in XR, we tracked the carotenoid-to-retinal EET process, demonstrated by the excess of signal amplitude, at very early times, at the EET related cross peak, and by possible hot-GS photo-absorption signals, overlapping with the previously mentioned ESA. Our analysis enables to explore the role played by the CAR ground state vibrational levels in controlling and promoting the CAR→RET EET efficiency.

The Results and Discussion section is organized as follows: first we introduce the Spectral Overlap (between CAR emission and RET absorption) as a mean to describe the probability to populate the different CAR GS vibrational levels following the CAR→RET energy transfer. Then we analyze the measured 2DES maps at few selected population times, enlightening additional evidences in favor of the ultrafast EET process. We discuss similarity and differences of 2DES and PP measurements, eventually summarizing the obtained results in a concise scheme (Figure 7).

Results and Discussion

The comparison between experimental absorption spectra of XR and RXR and the theoretical CAR absorption curve is shown in Figure 1, together with the experimental intensity spectra of the pulses employed in 2DES and PP measurements: the former overlaps only with the tail of the CAR S_2 transition, while the latter is resonant with excited vibrational levels of the same transition. As previously reported [9,14], the reduction of the retinal chromophore after $NaBH_4$ treatment produces a quenching in the absorption for wavelength longer than 450 nm, accompanied by an increase of the absorption below 450 nm. The difference between the XR and the RXR absorption (grey filled curve of Figure 1) therefore reveals, in this region of the spectrum, the retinal contribution to the overall XR absorption. The theoretical RXR absorption spectrum matches the experimental one in the red side of the considered window, while it is considerable less intense in the blue side, where reduced retinal contributions (not accounted for in the model) are present. Note also that the negligible shift of the CAR transitions in XR and RXR indicates

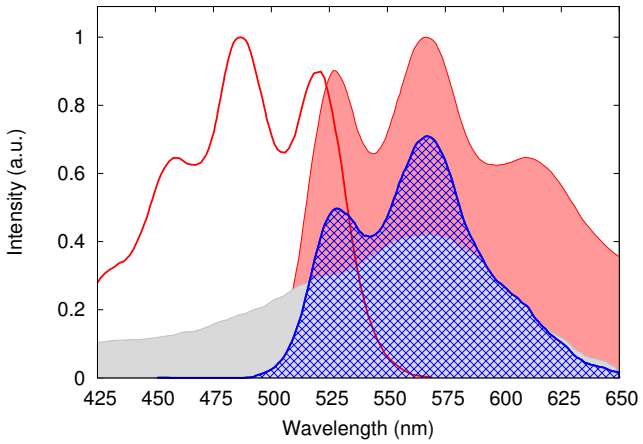

Figure 2. Experimental absorption spectra of RXR (red solid line) and its mirror image, representing the CAR S_2 fluorescence spectrum (red filled curve), together with RET absorption (grey filled curve). The Spectral Overlap, i.e. the integrand of Eq. (1), is depicted in blue. The experimental spectra were adapted from ref. 9.

that CAR and RET are not forming a delocalized exciton state, as they maintain their individuality in both samples. This is further corroborated by the observed retention of carotene chirality in circular dichroism spectra [21,22] of both XR and RXR [15].

This observation points toward a Förster EET mechanism between localized CAR and RET states, which was previously postulated for the XR system [14,23]. Förster resonant energy transfer theory provides the EET rate when the interaction between the chromophores and the so called spectral overlap integral are known. The spectral overlap integral is given by

$$J = \int F(\nu)A(\nu)/\nu^4 \; d\nu \quad (1)$$

where $F(\nu)$ and $A(\nu)$ are, respectively, the emission spectrum of the donor and the absorption spectrum of the acceptor (converted in energy scale and normalized to the unit area [24]). Figure 2 shows both the measured absorption of salinixanthin S_2 and its fluorescence, taken as the absorption mirror image [9], together with the computed spectral overlap.

The spectral overlap shown in Figure 2 (whose structure reflects the vibronic peaks of the CAR S_2 emission) allows for a qualitative estimate of the probability to populate the different possible CAR ground state (GS) vibrational levels following the CAR→RET energy transfer. In particular, we note that a large percentage of the excited CAR molecules will not repopulate the original (cold) GS, but rather (hot) excited vibrational states of it. This remains true also when the measured salinixanthin S_2 fluorescence spectrum, which extends less in the red than the absorption mirror image, is employed for the spectral overlap calculation (see Figure S1 of the SI). We remark here that it is not advisable to use the spectral overlap as a source of quantitative information. One should in fact consider that the CAR emission at very early times can differ from the CAR fluorescence profile, and can also be different when different pulse profiles are employed.

The analysis of the spectral overlap impacts the analysis of the experimental spectra in the following ways: i) the shape of the spectral overlap suggests that the maximum of the CAR-RET energy transfer related cross-peak in 2DES should appear around 520 nm pump and 560 nm probe. Moreover, as not all the excited CAR population involved in the energy transfer goes back to the vibrationally cold GS, one could observe ii) only a partial drop of the CAR GSB signal concurrent to energy transfer (i.e., not the expected 30-40% decay suggested by the EET efficiency, but just a fraction of it), and iii) the build-up of CAR hot GS photoinduced absorption signals in XR sample, which should appear as negative contributions at the red side of the 520 nm CAR GSB diagonal signal.

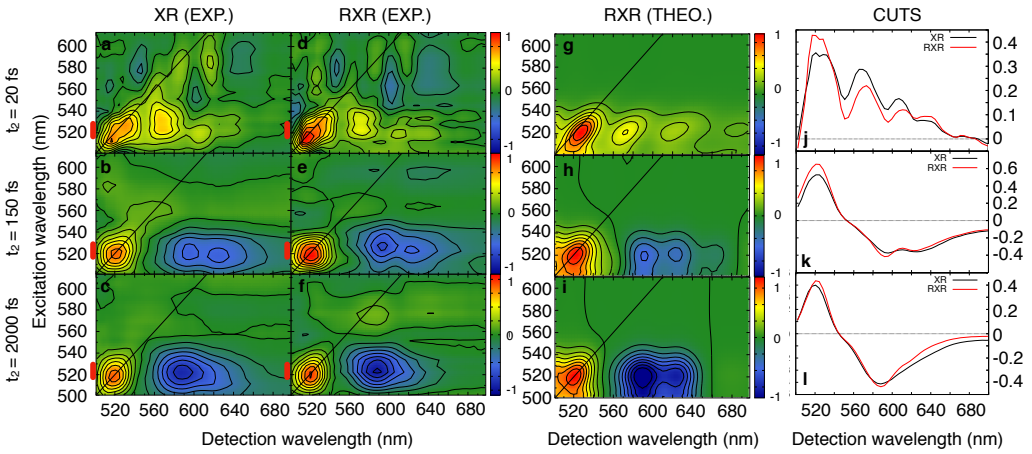

Figure 3. Experimental 2DES XR maps (a-c), experimental 2DES RXR maps (d-f), simulated RXR maps (g-i) and cuts of these maps (j-l) at different waiting times. The experimental maps were plotted between common XR and RXR values ([-maximum,maximum]) at every selected t_2 time. XR data were normalized so that, at t_2 ~ 400 fs, the CAR GSB intensity (at the 520 nm diagonal) is the 85% of the RXR CAR GSB intensity. Theoretical maps were normalized in the range [-maximum,maximum] (see Section S6 of the SI) at every waiting time t_2. The 2DES cuts were taken averaging the signal in the pump rage 515-530 nm (as highlighted by the red markers at the left side of the experimental maps).

All of that considered, and to take into account differences in the samples optical densities and in the experimental conditions, we chose to renormalize XR signals in both 2DES and PP data, so that the 520 nm CAR signal after 400 fs (to be interpreted mainly as CAR S0 GSB, as CAR S2 SE should have already decayed at this time delay) is 85% of that of RXR (assuming an EET efficiency of ~40% and that only ~40% of the CAR molecules involved in this process goes back to the original GS, as suggested by the area below the first peak of the blue spectra in Figure 2). The results presented hereafter are shown to be robust against a range of possible XR scaling factors, as discussed in Section S2 of the SI.

Figure 3 presents experimental 2DES maps at three selected waiting times (t2 = 20, 150, 2000 fs) for the XR and the RXR samples (Figure 3 a-f), together with simulated RXR maps (Figure 3 g-i) and cuts (Figure 3 j-l) of the 2DES maps obtained by averaging over a range of excitation wavelengths.

At t_2 = 20 fs (top row of Figure 3) the main detected signals in both samples are the positive GSB (diagonal peak at 520 nm) and SE (sequence of peaks from the diagonal to the red side of the spectrum) of the salinixanthin S_2 state, which lasts for a few tens of femtoseconds. The comparison of XR and RXR cuts reveals a remarkable difference: an excess of signal amplitude in the XR sample at the CAR-RET cross-peak (Figure 3j), directly revealing, as discussed afterwards, the presence of the underlying EET process. At t_2 times around 100-200 fs (central row in Figure 3) we observe the positive salinixanthin S_2 GSB band, which becomes more symmetric, from the initially elongated form, due to spectral diffusion, and the well-known negative salinixanthin S_1 (the elongated blue peak in the red side of Figure 3b, 3e and 3h) and S* (the blue peak around 585 nm probe in the same panels of Figure 3) ESA signals, in the interval 550-750 nm, which dominate and cover the carotenoid-retinal cross-peak and the CAR S_2 SE region. The comparison of the cuts (Figure 3k) shows an unexpected similarity of the ESA signals intensity in the two samples, in contrast with the notion that the RXR CAR S_1 (and S*) should have been populated more than in XR, being IC the unique deactivation channel for CAR S_2 in the former system. Following the analysis of the spectral overlap, the observation that a large percentage of the CAR molecules involved in the EET process will populate excited vibrational levels of the CAR GS, rather than the original cold GS, suggests a possible explanation of this similarity: photoinduced absorption from this vibrationally hot GS will indeed result in a negative signal that appears red-shifted with respect to the salinixanthin GS absorption (Figure 4c). This signal superimposes constructively with the negative S_1/S* ESA, and might explain the enhanced intensity of XR features in that spectral region. Furthermore, the ultrafast nature of the carotenoid-to-retinal EET process is also understood in terms of the improved energy resonance condition between the two molecules [25] which is guaranteed when the vibrational excited states of CAR GS are populated: this is clearly suggested by looking at the spectral overlap profile of Figure 2, which shows that the largest overlap between RET S_1 absorption and CAR S_2 emission involves the second vibronic band of the latter.

At longer times (t_2>1ps, bottom row in Figure 3) we still observe the carotenoid S_0 GSB signal on the diagonal and the S_1 (S*) ESA cross peak, which has been narrowed and blue-shifted due to S_1 vibrational cooling. In the XR complex, at this delay time, we also expect to see the photoinduced absorption signals of the J (and early populated K) photo-product state of RET as previously suggested by Polivka et al. [14], which is indeed revealed by the clear increase of signal in the XR cut.

In Figure 4, we present a comparison between experimental and theoretical differences of the XR and RXR cuts (obtained by averaging the signals in the 515-530 nm pump wavelength window) at early times (t_2 = 20 fs). The theoretical XR curve only considers CAR contributions, accounting for the shorter lifetime of the S_2 state due to the presence of the EET channel. We show that the prediction of a model which excludes both direct and indirect retinal contributions at pump wavelength corresponding to salinixanthin S_2 excitation (red dashed curve in Figure 4c), is qualitatively different with respect to experimental measurements (black solid curve in Figure 4c). On the contrary, the addition of a retinal-like GSB/SE contribution (modeled via a gaussian function centered around the retinal absorption maximum, the grey filled curve of Figure 4c), turns out to reproduce the main features of the XR/RXR difference. The introduced gaussian contribution represents a signal of the right sign (positive) and at the right position (EET related CAR-RET cross-peak) to qualitatively resemble a sensitized retinal GSB/SE signal. We assign to the EET related signal the excess of signal amplitude observed for the 520nm/560nm cross-peak in the XR sample. To support this assignment, we discuss in detail the origin of all the signals which could in principle contribute to this spectral region at early times, when pumping the carotene chromophore (between 510-530 nm) and probing in the 500-750 nm window.

The presence of possible carotene $S_2 \rightarrow S_{2n}$ ESA signals cannot be excluded, but to the best of our knowledge it has never been reported in studies of similar carotenoid systems in the visible

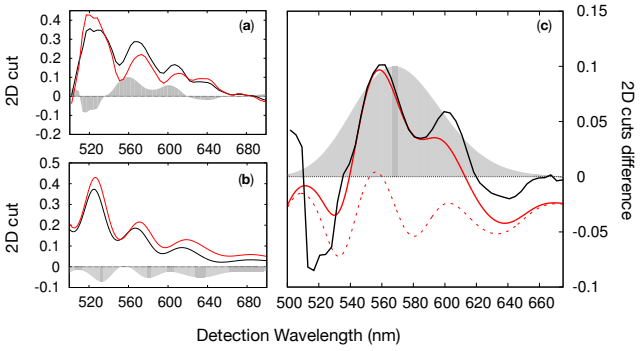

Figure 4. Differences of XR and RXR 2DES cuts obtained by averaging excitations wavelengths in the 515-530 nm interval at t_2 = 20 fs. Experimental (a) and theoretical (b) XR and RXR cuts (red and black solid line respectively) together with their differences (grey filled curves). Since in the theoretical maps RET contributions are not considered, the differences between the two curves are only given by the different S_2 states lifetimes (which control the S_2 SE disappearance, and produce the lifetime broadening of the transitions) and by the imposed XR CAR GSB scaling described in the main text (XR CAR GSB at 400 fs is the 85% of the RXR CAR GSB). Panel (c): experimental difference (black solid line) and theoretical difference, before (red dashed line) and after (red solid line) the sum with the retinal GSB/SE component (grey filled curve).

region (they are instead observed in the near-infrared region, around 1200 nm [15]). We exclude CAR $S_1 \rightarrow S_{1n}$ (and corresponding $S^* \rightarrow S^*_n$) ESA signals, which are known to appear only at later times. Contributions from direct retinal excitation (which has a non-negligible absorption at 520 nm) are also of minor importance: direct retinal contributions are barely detected, in 2DES maps, at the maximum of the retinal absorption (a very weak signal is measured in the diagonal around 560 nm, as shown in Figure S3 of the SI), being therefore even weaker for wavelengths around 520 nm at which the retinal absorbs less. At variance, indirect RET signals (i.e. signals coming from RET populated via EET from the CAR S2) are much more intense, as they are weighted with the CAR S2 dipole strength (see Section S4, SI). To this respect, we note that the ability of monitoring both direct and indirect (sensitized) RET signals in different spectral regions of the same recorded maps is a considerable advantage of 2DES over PP experiments.

One could expect to observe, due to the presence of a finite carotenoid-retinal coupling, cross-peaks in the CAR-RET off diagonal region, both above and below diagonal. We do not observe any signal in the above diagonal region, and we can exclude possible contributions also in the region of interest: due to the negligible delocalization of the excitation on the two chromophores we expect a cancelation of coupling related off-diagonal signals. It is worth noting that a fast disappearance of the XR-RXR differential signal at this (520-560 nm) cross-peak is also observed. This can be easily accounted for considering the underlying fast evolution of the retinal chromophore when promoted to its S_1 state by the EET process: in fact, if at short times the retinal SE (appearing during the carotene-to-retinal EET process) should be similar to the retinal GS absorption, it very quickly undergoes a pronounced red-shift, disappearing from the probed window, as previously observed for other rhodopsin systems in correspondence to isomerization [26,27]. Moreover, negative contributions from the salinixanthin S_1 (S^*) ESA will progressively gain intensity at increasing t_2 times, thus masking the cross peak (the evolution of the involved states is also reported in Figure 7d). All that in mind, it is apparent that the above described signals prove indirect excitation of the retinal chromophore via ultrafast EET from the carotene moiety that has been directly excited by light.

In Figure 5 we compare PP signals ("PP – 480" and "PP – 520", with pump pulses centered at 480 and 520 nm, respectively) and 2DES cuts (obtained by averaging the signals for excitation wavelengths between 500 and 550 nm) for both XR and RXR at early times. For each experiment, XR data were normalized as previously explained.

The 6 graphs look very similar, as they are all dominated by CAR related signals. In all the three experiments CAR S_2 GSB and S_1/S^* ESA signals are recorded, together with CAR S_2 SE, visible at 30 fs as a sequence of positive peaks in the 530-650 nm interval; one can also observe in all the samples an excess of signal intensity in the XR sample around 560 nm at 30 fs, here identified (also thanks to the ability of 2DES of resolving the signals over an additional -excitation- energy axis) as a signature of the CAR S_2 to RET S_1 EET.

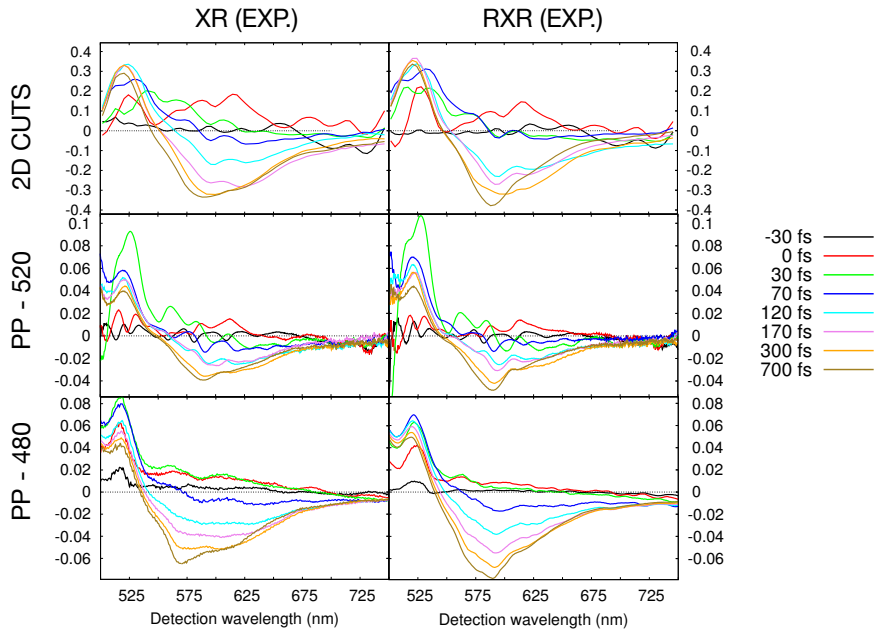

Figure 5. Comparison of XR (left column) and RXR (right column) experimental 2DES cuts and PP spectra at selected time delays. All the curves were normalized so that the XR CAR GSB at 400 fs is the 85% of the RXR CAR GSB, as described in the text. The data were plotted with a sign convention consistent with the one of the 2DES maps: GSB and SE signals are positive, while ESA signals are negative.

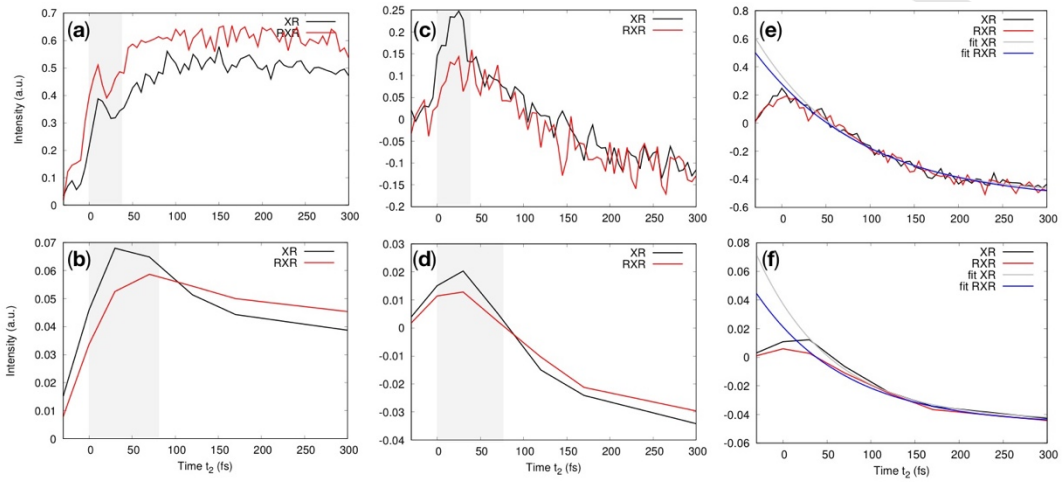

Figure 6. Evolution of selected regions of 2DES maps (first row) and PP data (second row) along the population time t_2. (a) 2DES region within 520-530 nm pump and 520-530 probe (CAR GSB and SE); (b) PP evolution at 520 nm; (c) 2DES region within 520-530 nm pump and 560 probe (CAR SE and EET cross-peak); (d) PP evolution at 560 nm; (e) 2DES region within 520-530 nm pump and 610 probe ($S_1 \rightarrow S_{1n}$ ESA); the fits give a build-up of the ESA peak with time constants of 108 fs and 127 fs for XR and RXR, respectively; (f) PP evolution at 615 nm; the fits give a build-up of the ESA peak with time constants of 85 fs and 102 fs for XR and RXR, respectively. The shadows highlight region of interest in the various plots. All the curves were normalized so that the XR CAR bleaching at 400 fs is the 85% of the RXR CAR bleaching, as described in the text.

Differences in the various experiments in the max/min ratio at each given time delay can be attributed to the different pulse polarization setups. We also note that the positioning of some peaks (e.g., CAR GSB and max of S1/S* ESA) is nearly the same for 2D cuts and PP – 520, while these are slightly blue-shifted in the PP – 480 XR sample. Finally, one of the most remarkable differences is related to the dynamics of the 520 nm peak (Figure 6(a-b)) in both PP data the signal increases, reaches a maximum (where CAR S2 GSB and SE constructively add together) and then quickly decays (due to the CAR SE decay), while in the 2DES the peak experiences a different dynamics, as if a negative signal was temporarily overlapping in that region. A similar dynamics of the peak was observed in ref. 18, for β-carotene, where a comparable pulse setup, overlapping with the red tail of the β-carotene absorption spectrum, was employed. There is no simple explanation why PP and 2DES signals obtained employing the same pulse shapes and polarizations should display different peaks dynamics. It has recently been demonstrated that the effect of the laser spectral profile on the observed spectral features in 2DES is highly non-trivial, and attention should be paid to avoid signal misinterpretation [28]. To this respect, the peculiar dynamics of the CAR 520 nm peak has to be further investigated. In Figure 6 we also report the evolution of the signal intensity in the 520 nm – 560 nm region (EET related cross-peak, Figure 6(c-d)), highlighting the excess of XR signal amplitude with a grey shadow, and in the 520 nm – 610 nm region ($S_1 \rightarrow S_{1n}$ signals, Figure 6(e-f)); the fits show that in both 2DES and PP data the build-up of this ESA signal is faster in XR than in RXR, as expected from the fact that the lifetime of the CAR S_2 state is shorter in the native system than in the reduced one. This represents another indirect proof of the occurrence of EET in XR. A comprehensive scheme of the states and the signals involved in a 2DES experiment on XR, is depicted in Figure 7, and it summarizes some of the obtained results: Figures 7(b) shows that the resonant donor-acceptor condition is enhanced by vibrationally excited levels of the GS of the donor (salinixanthin). Figure 7(c) shows both the red-shift of the RET emission over time, the $S_1 \rightarrow S_{1n}$ ($S^* \rightarrow S^*_n$) ESA following IC, and the hot CAR GS absorption following EET. Figure 7(e) summarizes the evolution of states population in both XR and RXR, as obtained within a simple rate equation model. The model includes the ultra-short signal lifetime of the "Franck-Condon" S_1 state of the retinal, set to 30 fs (following the arguments of ref. 26). The fast evolution of the RET on its potential energy surface, together with the emerging CAR S_1 (and S*) ESA signals, explains the fast disappearance of EET related RET signals around 560 nm in the 2DES maps.

Conclusions

In conclusion, we have compared 2DES and PP measurements performed on XR and RXR systems. The identification and interpretation of the recorded signals in both spectroscopic techniques, supported by a theoretical analysis, allowed us to provide additional evidence of the ultrafast carotenoid-to-retinal EET process at very early population times t_2. Interestingly, our analysis uncovers the importance of vibrationally excited levels of

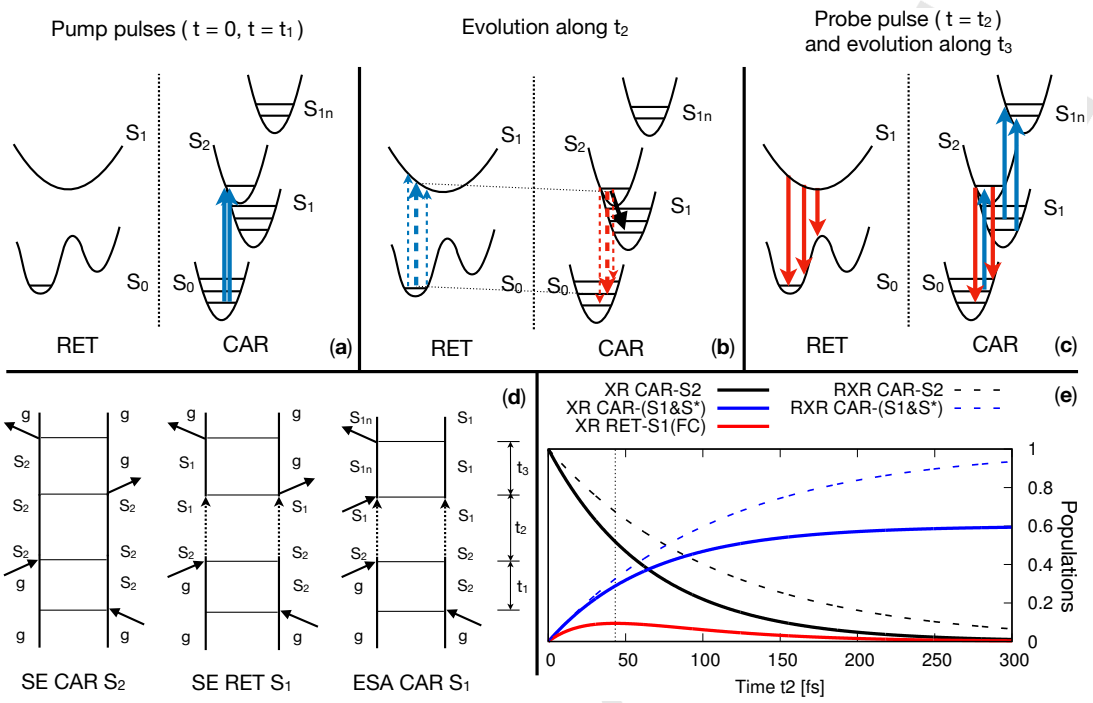

Figure 7. (a-c) Energy level diagrams depicting the main transitions occurring during times t_1, t_2 and t_3: (a) excitation of the salinixanthin S_2 state (the direct retinal excitation, which is a minor component, is not shown), (b) IC (black solid arrow) and EET (upwards and downwards dashed arrows) processes activated after excitation of salinixanthin in XR (the energy matching condition for EET is maximized when hot CAR GS vibrations are populated, as highlighted by the different arrow thickness), (c) main SE (both in CAR S_2 and in RET S_1), and ESA signals ($S_1 \rightarrow S_{1n}$); blue arrows denote absorption, while red arrows emission; only the S_1 state is shown for clarity (similar schemes hold for CAR S*), and for the same reason only one effective mode is depicted in the PES; (d) (Rephasing) Feynman diagrams of the possible processes activated after population of CAR S_2 state (a population preserving diagram, giving rise to S_2 SE, and two population changing diagrams, giving rise to EET related SE and IC related ESA); the dashed arrows indicate that population is changing during t_2. Similar considerations hold for non-rephasing diagrams. (e) Population dynamics of the spectroscopic relevant states in XR (solid lines) and RXR (dashed lines), for a model in which EET has ~40% efficiency.

the carotenoid electronic ground state in assisting the ultrafast CAR→RET EET process, as they provide improved energy matching and increased transition probability. This model is supported by the analysis of the CAR S_2 – RET S_1 spectral overlap, which suggests that during the energy transfer process the CAR S_0-S_2 GSB signal will not drop by the expected 30-40% (i.e., the efficiency of the EET process), but only by a fraction of it, eventually allowing to explain the presence of additional negative signals at the red side of the CAR S_2 bleaching as the absorption from a hot GS CAR to S_2. The impact of the different excitation pulse spectra on this analysis and on the interpretation of the recorded signals has to be further investigated.

Finally, we note that despite the simplicity of the system (a donor-acceptor couple), the obtained maps are highly congested by overlapping spectral features, and that theoretical modeling is needed for signals identification.

Experimental Section

Sample Preparation: XR protein was extracted from S. Ruber (the growth was carried out according to previously published methods [1]). XR membranes samples were isolated using previously described procedures [29]. The XR and RXR samples were prepared in 0.1 M NaCl and 50 mM Tris buffer, at pH = 8.4.

Reduction of the protonated Schiff-base bond with $NaBH_4$**:** To a solution of native XR (50 mM Tris buffer, pH = 8.4, 300 mM NaCl, 30% sucrose), 0.12 M of $NaBH_4$ were added. The reduction process was carried out using illumination for 1h. The light was filtered through a long pass cut-off filter with λmax> 550 nm (Schott, Mainz, Germany) to prevent over heating of the sample. The sample was dialyzed against 0.1 M NaCl, to remove $NaBH_4$.

PP setup: A room temperature sample was syringe pumped through a 0.4 mm path length flow cell equipped with 0.1 mm glass windows. The concentrations of XR and RXR in buffer produced nominal OD of 0.7 at 480 nm. The integrity of the sample was determined by measuring its absorption spectrum before and after each run. 30 fs pulses at 790 nm

were derived from a homemade multipass amplified Ti:Sapphire laser system. A few µJ were used to generate a multi-filament white light continuum probe by focusing in 3 mm of sapphire. The continuum pulses were collimated and re-focused into the sample with reflective optics. The remaining fundamental was used to pump an optical parametric amplifier (OPA, TOPAS, Light Conversion) and produce 30 fs pump pulses centered at 480 nm by mixing signal with OPA fundamental. The pump chirp was compensated in a slightly misaligned zero dispersion grating pulse shaper. 250 nJ of the resulting pulse was focused in the sample to a spot of ~200 um in diameter. Kerr scans in water provided the probes' wavelength dependent group delay, and indicated a pump–probe cross-correlation of ~70 fs throughout the probed range. After the sample, probe and reference pulses were collected by fibers into a double spectrometer setup to generate the time-dependent differential transmission spectra. The resulting spectra were corrected for group delay dispersion of the probe continuum.

2DES setup: The principle of operation of our 2DES setup is described extensively elsewhere [30,31]. 2DES in the partially linear pump-probe geometry can be seen as an extension of conventional PP spectroscopy, where two identical collinear pump pulses are used and their delay t_1 (coherence time) is scanned in time, for a fixed value of the probe pulse delay t_2 (population time). The probe pulse is dispersed in a spectrometer, providing resolution in the detection frequency. The Fourier transform with respect to the pump pulses delay provides the resolution of the signals with respect to the excitation frequency. The 2DES setup starts with a non-collinear OPA (NOPA) generating sub-10-fs visible pulses with spectrum extending from 500 to 720 nm. The NOPA output is divided by a beam splitter (90% transmission, 10 % reflection) into pump and probe lines. The identical and phase-locked pair of femtosecond pump pulses is generated by the Translating-Wedge-Based Identical-Pulses-eNcoding System (TWINS) technology [30,31]. TWINS uses birefringence to impose user-controlled temporal delays, with attosecond precision, between two orthogonal components of broad-bandwidth laser pulses. Rapid scanning of the inter-pulse delay allows robust and reliable generation of 2DES spectra. In order to determine zero delay between the pump pulses and properly phase the 2DES spectra, part of the pump beam is split off and sent to a photodiode to monitor the interferogram of the pump pulse pair. The additional dispersion introduced by the TWINS on the pump pulse pair is compensated by a suitable number of bounces on a pair of chirped mirrors. Pump and probe pulses are non-collinearly focused on the sample and the transient transmission change is measured on a CCD camera in a spectrometer. The polarization between pump and probe pulses was set to perpendicular with thin polarizers to minimize pump scattering signals on the CCD.

Theoretical Section

The electronic structure parameters of the S_2 state of the salinixanthin (CAR) moiety in both XR and RXR, were tuned to fit the red side of the experimental RXR absorption spectrum (less affected by the presence of the reduced retinal absorption). The main ingredients of the model include vertical excitation energy, transition dipole moment, and the strong intra-molecular C-C and C=C stretching modes (centred at 1155 cm^{-1} and 1520 cm^{-1}, respectively, in accordance with the Fourier analysis of XR spectral modulations [13]), responsible for the pronounced vibronic structure observed in the linear spectra (Figure 1). The lifetime of the Car S_2 state was accounted for, and set to 120 fs in the RXR (matching the S_2-to-S_1 internal conversion rate experimentally observed [14]) and to 70 fs in the XR (assuming a 40% efficiency for the carotenoid-to-retinal EET rate). Higher energy carotenoid excited states were also included in the model to reproduce the measured ESA signals ($S_1 \rightarrow S_{1n}$ and $S^* \rightarrow S^*_n$ transitions), and their parameters were fine-tuned to reproduce 2DES cuts at early times. All the model parameters are summarized in the SI (Tables S1, S2 and S3). The coupling of all the transitions to the continuum bath was also modeled through a spectral density (adapted from ref. 18), and the static disorder of the S_2 excitation energy was set to 260 cm^{-1}. In the simulation of 2DES maps, we have accounted for the finite time duration of the pulses by convoluting the maps (along t_2) with a gaussian function, whose width ($\sigma = 8$ fs) was determined as the time-width of the pulses. The pulse polarization was set to VVHH as in the experiment. A Stokes shift of 100 cm^{-1} for the RXR-CAR and 50 cm^{-1} for the XR-CAR, was applied to the simulated Stimulated Emission signals, to reproduce the 2DES cuts at early times.

Acknowledgements

This work was supported by the European Research Council Advanced Grant STRATUS (ERC-2011-AdG No. 291198) and the H2020 Grant Agreement number 765266 (LightDyNAmics).

Keywords: Two-Dimensional Electronic Spectroscopy • Förster Energy Transfer • ground state vibrations • Retinal Proteins • Carotenoids

[1] J. Antón, A. Oren, S. Benlloch, F. Rodríguez-Valera, R. Amann, R. Rosselló-Mora, *International Journal of Systematic and Evolutionary Microbiology* **2002**, 52(2), 485–491

[2] B. F. Lutnaes, A. Oren, S. Liaaen-Jensen, *Journal of Natural Products* **2002**, 65(9), 1340–1343

[3] T. Polívka, V Sundström, *Chemical Reviews* **2004**, 104(4), 2021-2072

[4] Y. Koyama, F. S. Rondonuwu, R. Fujii, Y. Watanabe, *Biopolymers* **2004**, 74(1-2), 2–18

[5] C. C. Gradinaru, J. T. M. Kennis, E. Papagiannakis, I. H. M. van Stokkum, R. J. Cogdell, G. R. Fleming, R. A. Niederman, R. van Grondelle, *Proceedings of the National Academy of Sciences* **2001**, 98(5), 2364–2369

[6] R. A. Mathies, S. W. Lin, J. B. Ames, W. T. Polland, *Annual Review of Biophysics and Biophysical Chemistry* **1991**, 20(1), 491–518

[7] R. Mathies, C. Brito Cruz, W. Pollard, C. Shank, *Science* **1988**, 240(4853), 777-779

[8] H. Luecke, B. Schobert, J. Stagno, E. S. Imasheva, J. M. Wang, S. P. Balashov, J. K. Lanyi, *Proceedings of the National Academy of Sciences* **2008**, 105(43), 16561–16565.

[9] S. P. Balashov, E. S. Imasheva, J. M. Wang, J. K. Lanyi, *Biophysical Journal* **2008**, 95(5), 2402 – 2414

[10] J. K. Lanyi, S. P. Balashov, *Biochimica et Biophysica Acta (BBA)* **2008**, 1777 (7-8), 684-688

[11] S. P. Balashov, E. S. Imasheva, V. A. Boichenko, J. Antón, J. M. Wang, J. K. Lanyi, *Science* **2005**, 309(5743), 2061–2064.

[12] V. A. Boichenko, J. M. Wang, J. Antón, J. K. Lanyi, S. P. Balashov, *Biochimica et Biophysica Acta (BBA) - Bioenergetics* **2006**, 1757(12), 1649 – 1656

[13] J. Zhu, I. Gdor, E. Smolensky, N. Friedman, M. Sheves, S. Ruhman, *The Journal of Physical Chemistry B* **2010**, 114(8), 3038–3045

[14] T. Polívka, S. P. Balashov, P. Chábera, E. S. Imasheva, A. Yartsev, V. Sundstr, *Biophysical Journal* **2009**, 96(6), 2268 – 2277.

[15] I. Gdor, I. Zhu, B. Loevsky, E. Smolensky, N. Friedman, M. Sheves and S. Ruhman, *Physical Chemistry Chemical Physics* **2011**, 13, 3782-3787

[16] T. Brixner, J. Stenger, H. M. Vaswani, M. Cho, R. E. Blankenship, G. R. Fleming, *Nature* **2005**, 434(7033), 625-628

[17] G. S. Schlau-Cohen, A. Ishizaki, G. R. Fleming, *Chemical Physics* **2011**, 386(1-3), 1-22

[18] N. Christensson, F. Milota, A. Nemeth, J. Sperling, H. F. Kauffmannm T. Pullerits, J. Hauer, *The Journal of Physical Chemistry B* **2009**, 113(51), 16409-16419

[19] E. Collini, C. Y. Wong, K. E. Wilk, P. M. G. Curmi, P. Brumer, G. D. Scholes, *Nature* **2010**, 463, 644-647

[20] F. Segatta, L. Cupellini, S. Jurinovich, S. Mukamel, M. Dapor, S. Taioli, M. Garavelli, B. Mennucci, *Journal of the American Chemical Society* **2017**, 139(22), 7558-7567

[21] E. S. Imasheva, S. P. Balashov, J. M. Wang, J. K. Lanyi, *The Journal of Membrane Biology* **2010**, 239(1-2), 95-104

[22] E. S. Koganov, V. Brumfeld, N. Friedman, M. Sheves, *The Journal of Physical Chemistry B* **2014**, 119(2), 456-464

[23] K. J. Fujimoto, S. Hayashi Journal of the American Chemical Society 2009, 131(40), 14152-14153

[24] T. Förster, Modern Quantum Chemistry, Vol III, Academic Press, New York, **1965**

[25] V. Perlík, J. Seibt, L. J. Cranston, R. J. Cogdell, C. N. Lincoln, J. Savolainen, F. Šanda, T. Mancal, J. Hauer, *The Journal of Chemical Physics* **2015**, 142(21), 212434

[26] K. C. Hasson, F. Gai, P. A. Anfinrud, *Proceedings of the National Academy of Sciences* **1996**, 93(26), 15124–15129.

[27] D. Polli, P. Altoè, O. Weingart, K. M. Spillane, C. Manzoni, D. Brida, G. Tomasello, G. Orlandi, P. Kukura, R. A. Mathies, M. Garavelli, G. Cerullo, *Nature* **2010**, 467, 440

[28] F. V. de A. Camargo, L. Grimmelsmann, H. L. Anderson, S. R. Meech, I. A. Heisler, *Physical Review Letters* **2017**, 118(3)

[29] E. S. Imasheva, S. P. Balashov, J. M. Wang, E. Smolensky, M. Sheves, J. K. Lanyi, *Photochemistry and Photobiology* **2008**, 84(4), 977-984

[30] J. Réhault, M. Maiuri, A. Oriana, G. Cerullo, *Review of Scientific Instruments* **2014**, 85, 123107

[31] D. Brida, C. Manzoni, G. Cerullo, *Optical Letters* **2012**, 37, 3027-3029

FULL PAPER

The carotenoid-to-retinal excitation energy transfer in xanthorhodopsin is time-resolved by pump-probe and two-dimensional electronic spectroscopy techniques. An excess of signal amplitude at the energy transfer related cross-peak, with respect to reduced xanthodhodopsin, is a direct evidence of the process.

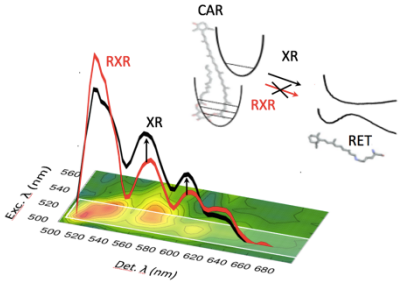

Francesco Segatta, Itay Gdor, Julien Réhault, Simone Taioli, Noga Friedman, Mordechai Sheves, Ivan Rivalta, Sanford Ruhman, Giulio Cerullo,* and Marco Garavelli**

Page No. – Page No.

Ultrafast Carotenoid to Retinal Energy Transfer in Xanthorhodopsin Revealed by the Combination of Transient Absorption and Two Dimensional Electronic Spectroscopy